

Interpretable Hybrid-Rule Temporal Point Processes

Yunyang Cao
Tongji University

Juekai Lin*
Tongji University

Hongye Wang*
Tongji University

Wenhao Li
Tongji University
whli@tongji.edu.cn

Bo Jin
Tongji University
bjin@tongji.edu

Abstract

Temporal Point Processes (TPPs) are widely used for modeling event sequences in various medical domains, such as disease onset prediction, progression analysis, and clinical decision support. Although TPPs effectively capture temporal dynamics, their lack of interpretability remains a critical challenge. Recent advancements have introduced interpretable TPPs. However, these methods fail to incorporate numerical features, thereby limiting their ability to generate precise predictions. To address this issue, we propose Hybrid-Rule Temporal Point Processes (HRTPP), a novel framework that integrates temporal logic rules with numerical features, improving both interpretability and predictive accuracy in event modeling. HRTPP comprises three key components: basic intensity for intrinsic event likelihood, rule-based intensity for structured temporal dependencies, and numerical feature intensity for dynamic probability modulation. To effectively discover valid rules, we introduce a two-phase rule mining strategy with Bayesian optimization. To evaluate our method, we establish a multi-criteria assessment framework, incorporating rule validity, model fitting, and temporal predictive accuracy. Experimental results on real-world medical datasets demonstrate that HRTPP outperforms state-of-the-art interpretable TPPs in terms of predictive performance and clinical interpretability. In case studies, the rules extracted by HRTPP explain the disease progression, offering valuable contributions to medical diagnosis. The code is available at <https://github.com/yy-c/HRTPP>.

Index Terms

Temporal Point Processes, Interpretability, Event Sequence Modeling, Logic Rules

I. INTRODUCTION

Event sequence data is prevalent in various domains, especially healthcare, including disease onset prediction [1], [2], progression analysis [3], [4], and clinical decision support [5], [6], where events occur asynchronously over time. Unlike traditional continuous-time series, which record values at regular intervals, event sequence data consists of discrete events with irregular time stamps, highlighting the necessity of specialized methods for discrete temporal data processing. Numerical features often accompany event sequences, providing crucial contextual information such as intensity, magnitude, or categorical attributes, which are essential for capturing complex temporal dependencies and enhancing predictive performance [7].

Temporal Point Processes (TPPs) are widely used for modeling event sequence data due to their ability to capture the stochastic nature of event occurrences over time. Traditional point process models, such as the Poisson process [8], Hawkes process [9], and self-correcting process [10], rely on predefined parametric intensity functions, which often struggle to capture complex temporal dependencies and require strong assumptions about the underlying data distribution. To address these limitations, neural point processes, including models based on recurrent neural networks (RNNs) [11], transformer architectures [12], and continuous normalizing flows [13], have been proposed to learn flexible, data-driven representations of event dynamics. However, these learning-based approaches often lack interpretability and require large amounts of training data to generalize effectively.

The interpretability of temporal point processes is crucial for many real-world applications, especially in healthcare, where understanding the underlying event dynamics is as important as making accurate predictions. For example, in medical diagnostics, an interpretable TPP model can assist doctors in analyzing disease progression by identifying key rules influencing the timing of medical events. Recent advancements have introduced interpretable TPPs, incorporating rule-based mechanisms [4], [14], [15] or sparse attention structures [16]. However, these methods typically sacrifice key advantages of numerical features, thereby limiting their ability to generate precise predictions. Thus, existing approaches face several limitations: traditional TPP models [9], [17], though capable of utilizing numerical features, often lack the flexibility to capture complex temporal dependencies; neural TPP models [11], though powerful, are typically considered black boxes with limited transparency; and interpretable models [4], [16], while offering some level of interpretability, often fail to incorporate rich numerical features effectively, reducing their predictive accuracy and rule reliability.

An urgent issue is ensuring both interpretability and accuracy. To address these issues, we propose Hybrid-Rule Temporal Point Processes (HRTPP), a novel framework that integrates rule-based mechanisms with numerical feature enhancement. HRTPP integrates three key intensity components: basic intensity, rule-based intensity, and numerical feature intensity, which together determine the overall intensity. The numerical feature intensity captures the influence of continuous-valued attributes.

* These authors contributed equally to this work.

The rule-based intensity encodes temporal dependencies through predefined logic rules, which are optimized via a structured rule mining process involving Bayesian optimization. The best rule set is finally selected by a two-stage mining strategy.

The **contributions** of this paper are as follows:

- A rule-guided numerical augmentation framework is proposed, integrating rule-based mechanisms with numerical features to enhance TPP modeling.
- A two-phase rule mining strategy is introduced to balance search space complexity and predictive performance.
- A comprehensive evaluation paradigm for interpretable temporal point process models is established, incorporating multiple criteria to assess both predictive performance and rule reliability.

II. RELATED WORK

1) *Temporal Point Process*: Temporal Point Process (TPP) models provide a probabilistic framework for capturing event sequences in continuous time. A key challenge in TPP research lies in designing intensity functions that are both expressive and interpretable. Efforts to improve interpretability in TPPs have led to the development of attention-based and rule-based approaches. Attention-based approaches such as SA-HP [18] and THP [12] incorporate self-attention mechanisms to capture long-range dependencies in event sequences. ITHP [19] further explains THP by algebraic operations. Although these methods improve flexibility, the trade-off between accuracy and interpretability remains an open problem. Rule-based TPP models focus on enhancing interpretability through structured rule sets. TLPP [20] first introduces logic rules to model event intensities. TELLER [14] introduces a principled approach to mine rules that explain temporal dependencies. Based on this, CLUSTER [4] and NS-TPP [21] design different deep neural network structures to accelerate rule mining. Clock Logic Neural Network (CLNN) [22] incorporates weighted clock logic formulas as rules to model event interactions. The recent trend in TPP research highlights the need to balance both explainable and effective aspects, integrating structured rule-based approaches with deep learning models for more explainable and effective event modeling.

2) *Rule Mining*: Rule mining focuses on automatically discovering logical rules from event sequence data to explain event occurrence patterns. Traditional methods for rule discovery primarily identify frequent patterns, but struggle with capturing temporal dependencies. Apriori [23] efficiently extracts frequent event sets but fails to model event order. Sequential pattern mining techniques, such as CM-SPADE [24] and VGEN [25], attempt to incorporate temporal orders but face difficulties in handling fine-grained timestamps. To overcome these limitations, TELLER [14] formulates rule discovery as a maximum likelihood problem to generate high quality rules, but requires a lot of computation. CLUSTER [4] introduces an iterative framework based on the EM algorithm to improve rule mining efficiency. NS-TPP [21] represents predicates and logic rules as vector embeddings and introduces a neural-symbolic framework for rule mining. Clock Logic Neural Network (CLNN) [22] utilizes weighted clock logic formulas to introduce three novel rule forms and incorporate numerical values into the rules. HyperLogic [26] proposes the integration of if-then logic rules within neural network architectures.

III. BACKGROUND

TPPs are widely used to interpret complex event sequences over time. For example, in ICU monitoring, physicians analyze the progression of symptoms and lab results to make decisions. Understanding the logic rules among medical events is crucial for accurate diagnosis and treatment. This section briefly reviews temporal point processes and temporal logic rules.

A. Temporal Point Processes

Temporal Point Process (TPP) is mathematically represented as a stochastic process $\{t_i\}_{i=1}^N$ where each $\{t_i\}$ denotes the timestamp of an event, and N is the number of observed events within a given time window. The core component of TPPs is the conditional intensity function $\lambda(t)$, which defines the instantaneous rate of event occurrence at time t , given the history $\mathcal{H}_t = \{t_1, t_2, \dots, t_{i-1}\}$:

$$\lambda(t|\mathcal{H}_t) = \lim_{\Delta t \rightarrow 0} \frac{\mathbb{P}(N(t + \Delta t) - N(t) = 1 | \mathcal{H}_t)}{\Delta t}. \quad (1)$$

This intensity function governs the likelihood of an event happening at a particular time. The overall behavior of a TPP is captured by the joint distribution of event times. By modeling $\lambda(t|\mathcal{H}_t)$, TPPs can describe a wide range of event patterns, including those influenced by past occurrences, external features, or domain-specific rules.

B. Temporal Logic Rules

Temporal logic rules consist of two parts: temporal predicates and relations. Define a set of temporal predicates as $\mathcal{X} = \{X_1, X_2, \dots, X_n, Y\}$, where each predicates X_u is an independent variable, Y is a target variable. Define a set of temporal relations as \mathcal{C} , which define how the variables are related over time. Logic rules are in the form of "if-then". A generalized temporal logic rule R can be expressed in the form:

$$R : C_i(\psi_1, \psi_2) \rightarrow Y, \quad (2)$$

Hybrid-Rule Temporal Point Processes (HRTPP)

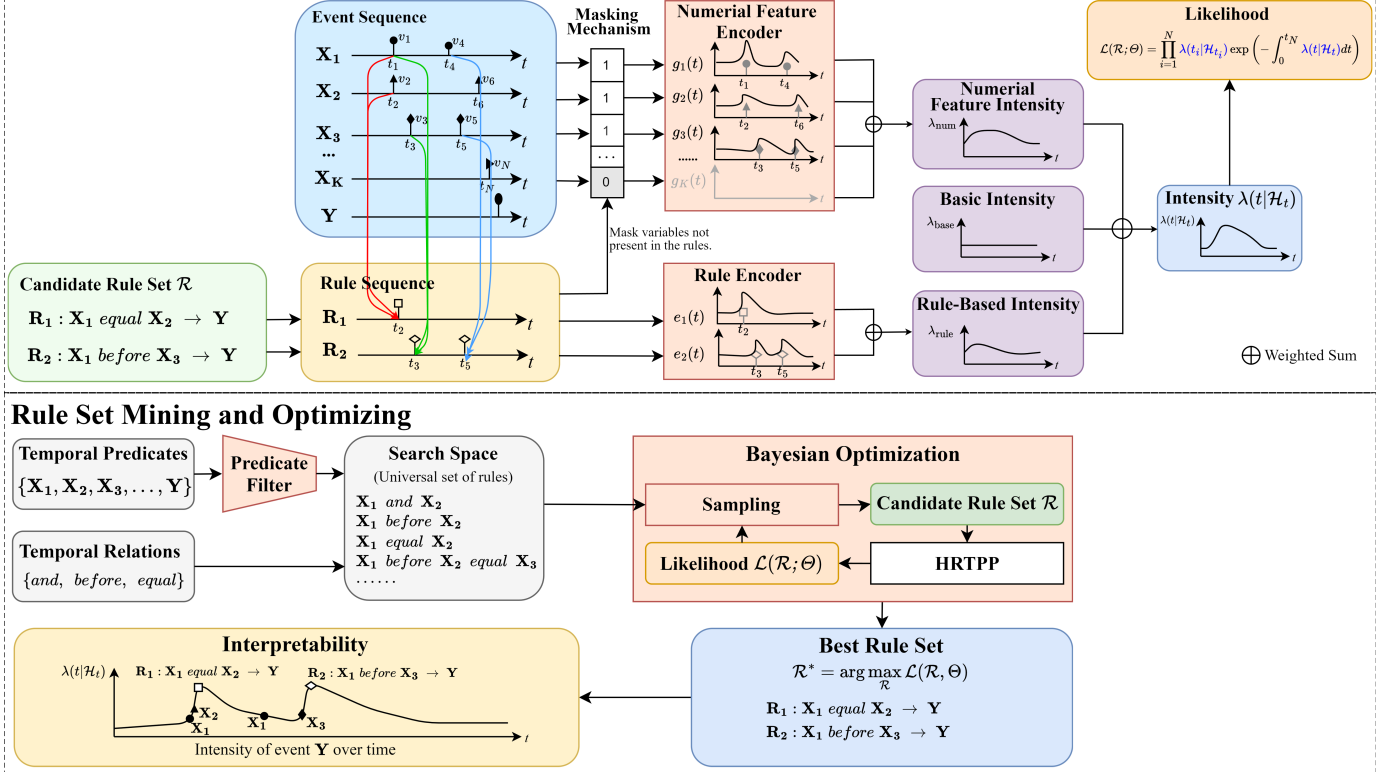


Fig. 1. The framework of model. In the HRTPP component, given a candidate rule set and event sequences, the model can compute the likelihood of the intensity function. The model integrates three key intensity components: basic intensity, rule-based intensity, and numerical feature intensity, which together determine the overall event intensity function $\lambda(t|\mathcal{H}_t)$. The numerical feature intensity captures the influence of continuous-valued attributes using a numerical feature encoder and a masking mechanism. The rule-based intensity encodes temporal dependencies through predefined rule set. In the rule set mining and optimizing component, Bayesian optimization iteratively refines the rule set by utilizing HRTPP computed likelihoods to guide the sampling distribution over the search space. The selected rules provide interpretable explanations of critical events via their impact on the intensity function dynamics.

where $C_i \in \mathcal{C}$ represents a temporal relation, and ψ_1, ψ_2 are expressions that can either be variables from \mathcal{X} or recursively defined temporal rules, such as X_u or ψ_u . The temporal relations between two temporal points can be divided into four types: *and*, *before*, *equal*, *after* [27]. Actually, " X_1 before X_2 " and " X_2 after X_1 " are equivalent, so the final set of temporal relations is $\mathcal{C} = \{\text{and}, \text{before}, \text{equal}\}$.

IV. METHODOLOGY

This section introduces the framework of Hybrid-Rule Temporal Point Processes (HRTPP), shown in Fig. 1. Given an event sequence $\mathcal{S} = \{(t_i, k_i, v_i)\}_{i=1}^N$ consisting of N events, each event type $k_i \in \{1, 2, \dots, K\}$ is associated with an independent variable X_{k_i} and a numerical feature v_i , providing contextual information. For instance, in ICU monitoring, an event k_i "elevated heart rate" at $t_i = 2$ hours may have $v_i = 120$ bpm. The conditional intensity function $\lambda(t|\mathcal{H}_t)$ is extended to incorporate temporal logic rules alongside numerical attributes, formulated as follows:

$$\lambda(t|\mathcal{H}_t) = f(\mathcal{S}_t; \Theta, \mathcal{R}), \quad (3)$$

where \mathcal{H}_t represents the historical event information, $\mathcal{S}_t = \{(t_i, k_i, v_i)\}_{t_i < t}$ denotes the observed event sequence, Θ is the set of model parameters, and \mathcal{R} comprises the extracted temporal logic rules that govern event dependencies.

A. Rule-Based Feature Construction

Temporal logic rules are essential in medical diagnosis, particularly in ICU monitoring, where capturing symptom progression is crucial for informed clinical decision-making. We propose a rule-based feature construction framework that integrates structured temporal rules with numerical features. This approach encodes event dependencies into numerical representations, ensuring a balance between explainability and data-driven modeling.

1) *Definitions of Temporal Rules:* Temporal rules formally define the logical relationships between different events over time, which consists of temporal predicates and temporal relations. In this study, we categorize the temporal relations between two time points into three types: *before*, *equal*, and *and*.

Given two predicates X_u and X_v with timestamps t_u and t_v , along with a target event Y occurring at $t_y > \max(t_u, t_v)$, the three types of temporal rules are mathematically defined as follows. *Before*, where X_u occurs before X_v within a small time tolerance δ , formulated as $C_{before}(X_u, X_v) = \mathbb{I}(t_u - t_v < -\delta)$. *Equal*, where X_u and X_v occur approximately at the same time, formulated as $C_{equal}(X_u, X_v) = \mathbb{I}(|t_u - t_v| \leq \delta)$. *And*, which simply states that both events occur without temporal constraints, formulated as $C_{and}(X_u, X_v) = 1$. Here, $\mathbb{I}(\cdot)$ represents the indicator function. These temporal rules provide a structured mechanism for capturing event dependencies.

2) *Rule Encoder:* To effectively incorporate temporal rules into the TPP framework, we encode hybrid-rule information into a continuous vector space. Based on the definitions of temporal rules, we construct hybrid-rule event sequences. For instance, consider the temporal rule " X_u before $X_v \rightarrow Y$ ". The corresponding hybrid-rule event sequence records the timestamps when the condition X_u before X_v is satisfied. Specifically, this sequence tracks each moment where the constraint $C_{before}(X_u, X_v)$ transitions from 0 to 1. The encoding function for a rule R_j is defined as:

$$e_j(t) = \sum_{t_j \in \mathcal{T}_j} d_{rule}(t - t_j), \quad (4)$$

where d_{rule} is the decay function, and \mathcal{T}_j denotes the set of timestamps when rule R_j is triggered. The choice of the decay function depends on real-world dynamics. For example, an exponential decay function, defined as $d_{rule}(t) = e^{-t}$ for $t \geq 0$, can model the diminishing influence of past rule activations over time.

3) *Numerical Feature Encoder:* Numerical features provides quantitative insight into the condition of a patient. Numerical feature encoder captures the dynamic influence of numerical attributes over time. Given an event sequence $\mathcal{S} = \{(t_i, k_i, v_i)\}_{i=1}^N$, the sequence corresponding to predicate X_k is expressed as $\{(t_i, k_i, v_i)\}_{k_i=k}$. However, not all predicates directly influence the target event. To address this, we introduce a masking mechanism to filter out irrelevant predicates. The mask is defined in accordance with the given rule set, where only predicates appearing in rules associated with the target event remain active. Formally, the mask set is denoted as $\mathcal{M} = \{m_k\}_{k=1}^K$, and the valid predicate set $\mathcal{X}_V \subset \mathcal{X}$ is defined as the collection of all variables appearing in the rules. The mask function is defined as $m_k = 1$ if $X_k \in \mathcal{X}_V$, and $m_k = 0$ otherwise. Using this masking mechanism and the sequence $\{(t_i, k_i, v_i)\}_{k_i=k}$, we define the numerical feature encoding function for predicate X_k as:

$$g_k(t) = m_k \sum_{i:k_i=k} v_i d_{num}(t - t_i), \quad (5)$$

where d_{num} is a time decay function, that models the influence of past numerical observations. The mask m_k ensures consistency within the HRTTP framework.

B. Hybrid-Rule Temporal Point Processes

HRTTP extends classical TPP by integrating rule-based dependencies and numerical features. The overall intensity function is composed of three key components. First, basic intensity models fundamental event patterns. Second, rule-based intensity encodes temporal logic rules. Third, numerical feature intensity incorporates clinical measurements to refine event prediction.

1) *Basic Intensity:* The basic intensity component λ_{base} captures the time independent information. This component reflects the inherent likelihood of events occurring. Mathematically, the basic intensity is expressed as: $\lambda_{base} = \lambda_0$, where λ_0 is a learnable parameter.

2) *Rule-Based Intensity:* The rule-based intensity component integrates domain expertise and temporal dependencies into the event modeling process. Given a predefined set of temporal rules \mathcal{R} , the rule-based intensity function is defined as:

$$\lambda_{rule}(t) = \sum_{R_j \in \mathcal{R}} \alpha_j e_j(t), \quad (6)$$

where α_j is a learnable parameter representing the weight associated with rule R_j . $e_j(t)$ denotes the encoding function, shown in Eq.(4). By incorporating rule-based intensity, HRTTP ensures that predictions align with medically interpretable dependencies rather than relying solely on data-driven patterns.

3) *Numerical Feature Intensity:* Numerical features such as heart rate and blood pressure provide an essential context for event predictions. The numerical feature intensity component modulates event occurrence probabilities based on these continuously valued attributes. The intensity function is defined as:

$$\lambda_{num}(t) = \sum_{k=1}^K \beta_k g_k(t), \quad (7)$$

where β_k is a learnable parameter representing the weight associated with predicate X_k . $g_k(t)$ is the numerical feature encoder, which is shown in Eq.(5). For example, if a patient's blood pressure remains high, it may increase the likelihood of a hypertension-related event. The numerical feature dynamically modulates event probabilities, providing a richer representation of patient status.

The overall intensity function integrates all three intensity components. In order to ensure that the overall intensity function remains positive, we apply the softplus transformation. The softplus function is defined as: $\text{Softplus}(x) = \gamma \log(1 + \exp(x/\gamma))$, where $\gamma > 0$ is a learnable parameter. By incorporating Eqs.(4)-(7), the final expression for the overall intensity function is as follows:

$$\begin{aligned} \lambda(t|\mathcal{H}_t) &= \text{Softplus}(\lambda_{\text{base}}(t) + \lambda_{\text{rule}}(t) + \lambda_{\text{num}}(t)) \\ &= \text{Softplus}\left(\lambda_0 + \sum_{R_j \in \mathcal{R}} \alpha_j \sum_{t_j \in \mathcal{T}^j} d_{\text{rule}}(t - t_j) + \sum_{k=1}^K \beta_k m_k \sum_{i:k_i=k} v_i d_{\text{num}}(t - t_i)\right). \end{aligned} \quad (8)$$

where $\Theta = \{\alpha, \beta, \gamma, \lambda_0\}$ is learnable parameters set, $\alpha = \{\alpha_j\}_{j=1}^{|\mathcal{R}|}$ is the set of weights associated with temporal rules, $\beta = \{\beta_i\}_{i=1}^K$ is the set of weights associated with numerical features. This overall intensity function serves as the foundation for modeling event occurrences in HRTTP framework, enabling robust modeling in event prediction and rule mining.

C. Training and Prediction

To effectively learn the parameters of the HRTTP model and enable accurate event prediction, we design a training framework based on likelihood maximization and employ our learned intensity function for future event forecasting.

1) *Loss Function:* The HRTTP model is trained by maximizing the likelihood of observed event sequences under the temporal point process framework. Given a event sequence $\mathcal{S} = (t_i, k_i, v_i)_{i=1}^N$ and rule set \mathcal{R} , the likelihood function is formulated as $\mathcal{L}(\Theta) = \prod_{i=1}^N \lambda(t_i|\mathcal{H}_{t_i}) \exp\left(-\int_0^{t_N} \lambda(t|\mathcal{H}_t) dt\right)$, where Θ is the set of learnable model parameters. To facilitate optimization, we minimize the negative log-likelihood (NLL) as the loss function:

$$\mathcal{L}_{\text{NLL}}(\Theta) = -\sum_{i=1}^N \log \lambda(t_i|\mathcal{H}_{t_i}) + \int_0^{t_N} \lambda(t|\mathcal{H}_t) dt. \quad (9)$$

This loss function ensures that the model learns to assign higher intensities to observed events while also maintaining proper event distributions over time.

2) *Event Prediction:* HRTTP model can be used to predict the timing of future events based on the learned intensity function. Given a history \mathcal{H}_t up to time t , the next event time \hat{t} is sampled from the conditional density function:

$$p(\hat{t}|\mathcal{H}_t) = \lambda(\hat{t}|\mathcal{H}_t) \exp\left(-\int_t^{\hat{t}} \lambda(s|\mathcal{H}_s) ds\right). \quad (10)$$

By minimizing the loss function, HRTTP effectively learns the underlying intensity function of event occurrences. By predicting the timing of the next event, HRTTP can capture the evolving dynamics of the sequence, offering valuable insights and data-driven support for medical diagnosis.

D. Rule Mining and Optimization

To efficiently extract temporal logic rules, a two-phase rule mining strategy is employed, incorporating rule candidate generation and Bayesian optimization.

1) *Rule Candidate Generation:* Temporal rules are derived from historical event sequences to construct a structured search space. Without constraints, the combination of predicates and relations can be excessively large. To address this, rule length is restricted, and predicate filtering is applied. Firstly, rule length significantly impacts interpretability. Overly complex rules hinder comprehension, whereas single-predicate rules lack temporal expressiveness. Based on medical guidelines, a maximum of two or three predicates is imposed. Secondly, predicate filtering is conducted via pre-training using a rule-free TPP model as a baseline. Each predicate is evaluated individually, and those reducing model loss are retained. The resulting filtered predicates are used to generate candidate rules, ensuring that each rule contains at least one valid predicate. This process refines the search space, facilitating efficient rule selection.

2) *Rule Optimization via Bayesian Optimization*: Following candidate generation, Bayesian optimization is utilized to refine the rule set and maximize predictive performance, avoiding the infeasibility of exhaustive searches. The objective is to identify the optimal rule subset \mathcal{R}^* that maximizes the model log-likelihood:

$$\mathcal{R}^* = \arg \max_{\mathcal{R}} \log \mathcal{L}(\mathcal{R}; \Theta), \quad (11)$$

where $\log \mathcal{L}(\mathcal{R}; \Theta)$ denotes the model likelihood given the rule set \mathcal{R} . To maintain efficiency and interpretability, the rule set size $|\mathcal{R}|$ is constrained.

Bayesian optimization iteratively updates the rule set in three steps: (1) sampling candidate subsets using a probabilistic acquisition function, (2) evaluating model performance, and (3) refining the posterior distribution to guide further searches. This approach efficiently identifies high-quality rules while mitigating overfitting and redundancy, ensuring an optimal balance between model accuracy and interpretability. Unlike brute-force search methods, Bayesian optimization efficiently explores the parameter space.

V. EXPERIMENTS

A. Experimental Setup

Datasets. We use four real-world disease-specific datasets: AKI (Acute Kidney Injury), Stroke, Sepsis, and CAD (Coronary Artery Disease). These medical datasets are extracted from MIMIC-IV [28], a large-scale medical database that contains electronic health records. Table I presents the statistical information of these datasets. As shown in the table, these four datasets increase in size from top to bottom. In the AKI dataset, disease progression to Phase III serves as the target event. The Stroke dataset focuses on patients transitioning from moderate to severe conditions. In the Sepsis dataset, the occurrence of low urine output is tracked as a target of organ failure. The CAD dataset defines patient mortality as the target event.

Baselines. We choose three state-of-the-art TPP models that are capable of rule mining.

TEmporal Logic rule LearnER (TELLER) [14]: This model can discover temporal logic rules by rule-extension-first-search or rule-addition-first-search.

Clock Logic Neural Network (CLNN) [22]: This model introduces a time-aware framework to provide weighted clock logic formulas as rules.

CLUSTER [4]: This model automatically extracts "if-then" logic rules to interpret observational events.

Evaluation Metrics. To assess the performance of the models, we conducted comprehensive experiments. Each dataset is split into an 80% training set and a 20% test set. The evaluation metrics used to measure predictive performance include *Negative Log-Likelihood (NLL)*, *Root Mean Squared Error (RMSE)* and *Rule Accuracy (Acc)*. Rule accuracy means the proportion of correct rules.

TABLE I
DATASETS STATISTICS.

Dataset	Sequences	Types	Events	Seq. Length	Avg. Length
AKI	2327	38	58k	[3, 123]	24.93
Stroke	4951	48	447k	[2, 2207]	97.47
Sepsis	20081	66	1375k	[2, 1406]	68.46
CAD	12459	56	3519k	[6, 7955]	282.45

B. Performance Analysis

In this section, we compare the performance of model fitting, event occurrence time prediction, and rule accuracy using three evaluation metrics. The results shown in Table II demonstrate that HRTPP outperforms baseline models. The lowest NLL indicates that HRTPP effectively captures and models uncertainty. HRTPP also achieves the lowest RMSE, suggesting precise event time predictions and enhancing reliability in medical applications. High rule accuracy of HRTPP demonstrates the extraction of medically relevant rules, improving interpretability and supporting transparent decision-making.

C. Rule Analysis

In this section, we analyze the quality of the rules from the perspectives of rule expression, correctness, reliability, and distribution, thereby verifying the interpretability of the model. We take the CAD dataset as an example. Fig. III shows top 10 rules of four models. The full rule results for the four datasets are shown in the Appendix.

TABLE II
COMPARISONS OF MAIN RESULTS.

	AKI			Stroke			Sepsis			CAD		
	NLL↓	RMSE↓	Acc↑	NLL↓	RMSE↓	Acc↑	NLL↓	RMSE↓	Acc↑	NLL↓	RMSE↓	Acc↑
TELLER	12.9	8.1	80%	21.8	8.4	100%	23.4	4.4	75%	203.8	5.3	80%
CLNN	277.5	10.4	83%	178.9	13.2	70%	207.2	5.9	67%	177.1	4.2	71%
CLUSTER	79.0	10.4	60%	36.3	13.2	65%	37.5	8.8	65%	98.9	10.4	55%
HRTTP	7.4	5.4	100%	15.1	4.3	100%	12.7	2.7	80%	5.8	3.7	100%

1) *Rule Expression Analysis*: In the CAD dataset, we set mortality as the target variable and compare HRTTP with baseline models. We refer to medical guidelines [29] to determine the correctness of the rules. Table III shows the rules, weights, and correctness. From the experimental results, TELLER and CLNN rely on simple variables and discover few rules, missing complex physiological interactions. CLUSTER offers more flexible rules but is highly sensitive to noise, making it difficult to extract correct medical indicators. In contrast, HRTTP uncovers clinically meaningful rules, such as 'if a high anion gap occurs before low heart rate, then death occurs', highlighting the link between metabolic disorders and circulatory failure. These rules enhance accuracy and align with medical logic, aiding clinical decision-making.

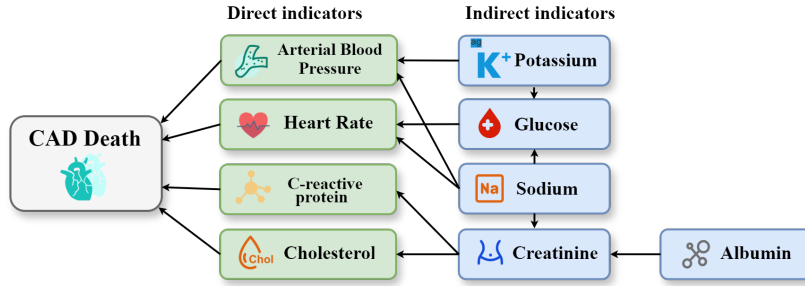


Fig. 2. Hierarchical relationships of CAD indicators. The indicators in green boxes are direct indicators, and those in blue boxes are indirect indicators. Arrows denote dependencies between indicators in a cause-effect manner.

2) *Rule Distribution Analysis*: Understanding mortality risk indicators in CAD patients is crucial for better management and prediction. To analyze these factors, we created a graph network based on medical guidelines [29], visually mapping their hierarchical relationships in Fig. 2. As shown in the Fig. 2, arterial blood pressure, heart rate, C-reactive protein and cholesterol directly effect mortality, while other indicators influence mortality through them. Hence, we classify the rules into direct or indirect rules according to their relationships. Table III shows direct indicators in green and indirect indicators in blue. HRTTP identifies the most direct rules, showing strong ability in capturing key CAD mortality factors. HRTTP also balances direct and indirect rules well, focusing on major factors without omitting minor details, thus enhancing its applicability in medical decision-making.

D. Stability Analysis

Model stability is crucial in medical decision support, ensuring consistency across conditions. To evaluate model stability, we recorded the frequency of four direct CAD indicators in five runs. Fig. 3 presents the results, where HR, ABP, Cho, and CRP denote Heart Rate, Arterial Blood Pressure, Cholesterol, and C-reactive Protein, respectively. As shown in the figure, HRTTP has the highest frequency of direct rules, which shows the best stability and consistency. Clinically, its stability ensures interpretable results by minimizing fluctuations caused by minor data changes, thereby enhancing decision-making accuracy and supporting personalized treatment.

E. Case Study

In this section, we show the mechanism by which rules and events affect the target. When a rule is triggered, its strength increases instantaneously, reflecting the potential risk associated with the condition. Fig. 4 shows the intensity curve of a CAD patient. In this figure, abnormalities in physiological indicators triggered key rules over time. At 17.19h, high blood glucose and creatinine appeared, followed by infection-related signs, increasing rule strength. At 60.26h, metabolic imbalance was triggered by an elevated anion gap and low heart rate. At 92.43h, high INR and low heart rate indicated coagulation abnormalities. Finally, at 123.58h, decreased oxygen saturation and increased blood pressure triggered the end-event rule, leading to a sharp rise in intensity and death.

TABLE III
RULES ON THE CAD DATASET.

Note: The predicates in green boxes are direct indicators, and those in blue boxes are indirect indicators.

Model	Rule	Weight	Correctness
TELLER	Respiratory Rate High \rightarrow Dead	0.2859	Correct
	Arterial Blood Pressure diastolic Low \rightarrow Dead	0.2202	Correct
	Heart Rate High \rightarrow Dead	0.1614	Correct
	Arterial Blood Pressure mean Low \rightarrow Dead	0.1400	Correct
	O2 saturation pulseoxymetry Low \rightarrow Dead	0.1283	Incorrect
CLNN	c_Glucose High - c_Death > -0.25	1.03	Correct
	c_BUN High - c_Death > -0.63	1.01	Correct
	c_INR Low - c_BUN High > 0.01	0.99	Incorrect
	c_Glucose High - c_AST Low > -0.08	0.99	Incorrect
	c_Albumin High - c_Glucose High > 0.02	0.97	Correct
	c_BUN High - c_C-Reactive-Protein High > -0.14	0.96	Correct
	c_Brain Natriuretic Peptide High - c_BUN High > 0.41	0.94	Correct
CLUSTER	BUN Low equal Lactic Acid Low	-	Incorrect
	Hemoglobin High equal Hematocrit High	-	Incorrect
	Brain Natriuretic Peptide High after ALT Low	-	Correct
	Heart Rate High before AST Low	-	Correct
	Calcium ionized High equal Total Bilirubin High	-	Incorrect
	CK-MB fraction High equal Calcium ionized Low	-	Correct
	Calcium ionized Low equal Cholesterol High	-	Correct
	Temperature Low equal Hemoglobin High	-	Correct
Hematocrit Low equal Total Bilirubin Low	-	Incorrect	
Glucose Low before Anion gap Low	-	Incorrect	
HRTPP	Heart Rate Low equal Arterial Blood Pressure diastolic High \rightarrow Dead	2.4073	Correct
	Anion gap High before Heart Rate Low \rightarrow Dead	1.7742	Correct
	Heart Rate Low equal Potassium High \rightarrow Dead	1.6257	Correct
	Potassium Low before O2 saturation pulseoxymetry Low \rightarrow Dead	1.3959	Correct
	Respiratory Rate Low before Potassium High \rightarrow Dead	1.1533	Correct
	Arterial Blood Pressure mean Low before Arterial Blood Pressure diastolic Low \rightarrow Dead	1.1312	Correct
	Anion gap Low equal O2 saturation pulseoxymetry Low \rightarrow Dead	1.1303	Correct
	Glucose Low equal Arterial Blood Pressure systolic Low \rightarrow Dead	0.5603	Correct
	Heart Rate Low equal INR High \rightarrow Dead	0.4213	Correct
	Temperature High and Respiratory Rate High \rightarrow Dead	0.3194	Correct

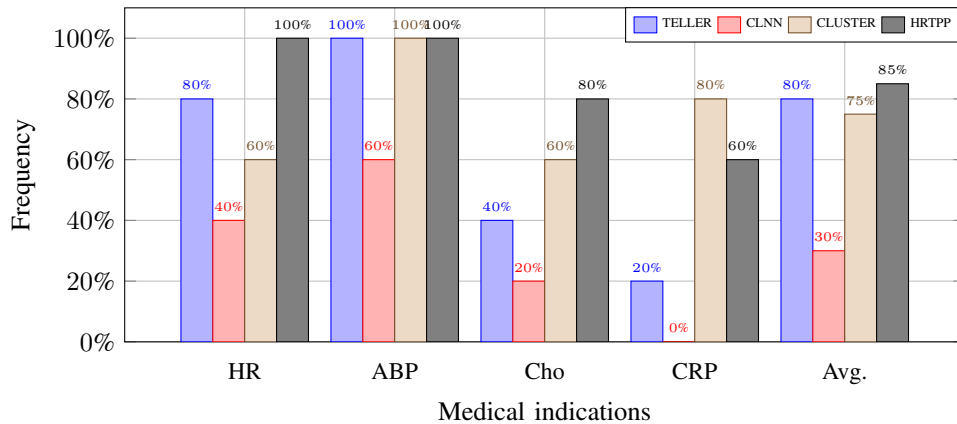


Fig. 3. Frequency of direct rules in five runs.

This mechanism enables real-time monitoring and early warning of high-risk conditions while providing interpretable analysis of disease progression to support clinical decisions. By applying rule-guided dynamic analysis, we identify key causal relationships in CAD progression and detect turning points in disease deterioration, allowing clinicians to intervene precisely at critical moments. These rules are not just data-driven predictions but verifiable medical reasoning, ensuring transparency and reliability in decision-making while improving the efficiency and accuracy of CAD diagnosis and treatment.

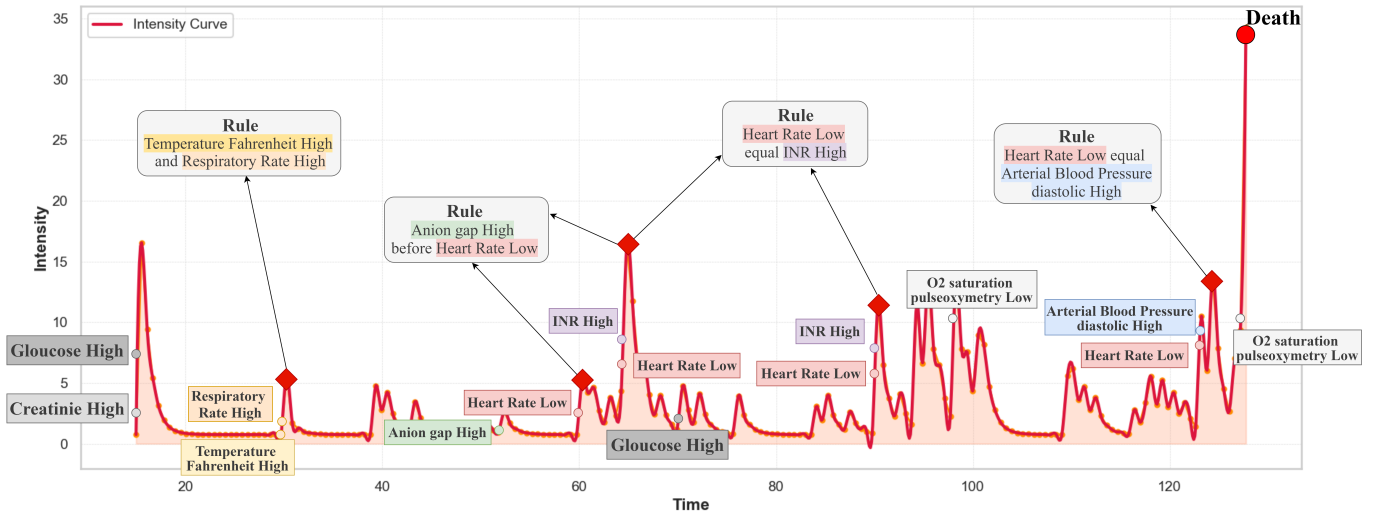


Fig. 4. Intensity over time for a CAD patient. The red curve represents the intensity of the target variable, reflecting the probability of death. Key events affecting the mortality are annotated below the curve, while the timing of logic rules is marked above. The entire figure illustrates the patient’s full clinical progression in the ICU.

F. Ablation Study

We conducted an ablation study on four datasets to assess the impact of Numerical Feature Augmentation (NFA) on model performance. We classify models into two categories. Category I uses only basic intensity, like probabilistic TPP models. Category II uses basic and rule-based intensity. Table IV shows the NLL of two categories. The experimental results indicate that incorporating NFA significantly improves model performance. These findings validate the effectiveness of numerical intensity in medical event modeling.

TABLE IV
ABLATION STUDY OF NUMERICAL FEATURE AUGMENTATION.

Category	State	AKI	Stroke	Sepsis	CAD
Category I	w/o NFA	7.41	15.26	12.83	6.30
	with NFA	7.41	15.24	12.73	5.96
Category II	w/o NFA	7.43	15.26	12.77	6.12
	with NFA	7.43	15.14	12.72	5.84

VI. CONCLUSION

This paper proposes Hybrid-Rule Temporal Point Processes (HRTTP), a novel framework that integrates rule-based reasoning with numerical feature modeling. The proposed approach effectively incorporates domain expertise through temporal logic rules, while leveraging numerical feature encoder to capture complex event dependencies. By integrating a structured rule mining and optimization strategy, HRTTP refines the rule search process, ensuring both efficiency and robustness in modeling event sequences. Experimental results demonstrate that HRTTP achieves superior predictive accuracy and interpretability compared to baseline methods, making it a valuable tool for medical diagnosis. Future work will focus on adaptive rule learning mechanisms to improve flexibility and generalization.

REFERENCES

- [1] Z. Che, S. Purushotham, K. Cho, D. Sontag, and Y. Liu, “Recurrent neural networks for multivariate time series with missing values,” *Scientific Reports*, vol. 8, no. 1, p. 6085, 2018.
- [2] P. Renc, Y. Jia, A. E. Samir, J. Was, Q. Li, D. W. Bates, and A. Sitek, “Zero shot health trajectory prediction using transformer,” *NPJ Digital Medicine*, vol. 7, no. 1, p. 256, 2024.
- [3] Z. Fan, J. Jiang, C. Xiao, Y. Chen, Q. Xia, J. Wang, M. Fang, Z. Wu, and F. Chen, “Construction and validation of prognostic models in critically ill patients with sepsis-associated acute kidney injury: Interpretable machine learning approach,” *Journal of Translational Medicine*, vol. 21, no. 1, p. 406, 2023.
- [4] Y. Kuang, C. Yang, Y. Yang, and S. Li, “Unveiling latent causal rules: A temporal point process approach for abnormal event explanation,” in *International Conference on Artificial Intelligence and Statistics*. PMLR, 2024, pp. 2935–2943.
- [5] N. Hayat, K. J. Geras, and F. E. Shamout, “Medfuse: Multi-modal fusion with clinical time-series data and chest x-ray images,” in *Machine Learning for Healthcare Conference*. PMLR, 2022, pp. 479–503.

- [6] J. Palma, J. M. Juarez, M. Campos, and R. Marin, "Fuzzy theory approach for temporal model-based diagnosis: An application to medical domains," *Artificial Intelligence in Medicine*, vol. 38, no. 2, pp. 197–218, 2006.
- [7] Z. Meng, B. Li, X. Fan, Z. Li, Y. Wang, F. Chen, and F. Zhou, "Transfeat-tpp: An interpretable deep covariate temporal point processes," *arXiv preprint arXiv:2407.16161*, 2024.
- [8] D. W. Jorgenson, "Multiple regression analysis of a poisson process," *Journal of the American Statistical Association*, vol. 56, no. 294, pp. 235–245, 1961.
- [9] A. G. Hawkes, "Spectra of some self-exciting and mutually exciting point processes," *Biometrika*, vol. 58, no. 1, pp. 83–90, 1971.
- [10] V. Isham and M. Westcott, "A self-correcting point process," *Stochastic Processes and Their Applications*, vol. 8, no. 3, pp. 335–347, 1979.
- [11] N. Du, H. Dai, R. Trivedi, U. Upadhyay, M. Gomez-Rodriguez, and L. Song, "Recurrent marked temporal point processes: Embedding event history to vector," in *Proceedings of the 22nd ACM SIGKDD Conference on Knowledge Discovery and Data Mining*, 2016, pp. 1555–1564.
- [12] S. Zuo, H. Jiang, Z. Li, T. Zhao, and H. Zha, "Transformer hawkes process," in *International Conference on Machine Learning*. PMLR, 2020, pp. 11 692–11 702.
- [13] G. Yang, X. Huang, Z. Hao, M.-Y. Liu, S. Belongie, and B. Hariharan, "Pointflow: 3d point cloud generation with continuous normalizing flows," in *Proceedings of the IEEE/CVF International Conference on Computer Vision*, 2019, pp. 4541–4550.
- [14] S. Li, M. Feng, L. Wang, A. Essofi, Y. Cao, J. Yan, and L. Song, "Explaining point processes by learning interpretable temporal logic rules," in *International Conference on Learning Representations*, 2021.
- [15] K. Walzer, A. Schill, and A. Löser, "Temporal constraints for rule-based event processing," in *Proceedings of the ACM first Ph. D. Workshop in CIKM*, 2007, pp. 93–100.
- [16] Z. Li and M. Sun, "Sparse transformer hawkes process for long event sequences," in *Joint European Conference on Machine Learning and Knowledge Discovery in Databases*. Springer, 2023, pp. 172–188.
- [17] A. Di Crescenzo, B. Martinucci, and S. Zacks, "Compound poisson process with a poisson subordinator," *Journal of Applied Probability*, vol. 52, no. 2, pp. 360–374, 2015.
- [18] Q. Zhang, A. Lipani, O. Kirnap, and E. Yilmaz, "Self-attentive hawkes process," in *International Conference on Machine Learning*. PMLR, 2020, pp. 11 183–11 193.
- [19] Z. Meng, K. Wan, Y. Huang, Z. Li, Y. Wang, and F. Zhou, "Interpretable transformer hawkes processes: Unveiling complex interactions in social networks," in *Proceedings of the 30th ACM SIGKDD Conference on Knowledge Discovery and Data Mining*, 2024, pp. 2200–2211.
- [20] S. Li, L. Wang, R. Zhang, X. Chang, X. Liu, Y. Xie, Y. Qi, and L. Song, "Temporal logic point processes," in *International Conference on Machine Learning*. PMLR, 2020, pp. 5990–6000.
- [21] Y. Yang, C. Yang, B. Li, Y. Fu, and S. Li, "Neuro-symbolic temporal point processes," in *International Conference on Machine Learning*, 2024.
- [22] R. Yan, Y. Wen, D. Bhattacharjya, R. Luss, T. Ma, A. Fokoue, and A. A. Julius, "Weighted clock logic point process," in *International Conference on Learning Research*, 2023.
- [23] R. Agrawal and R. Srikant, "Fast algorithms for mining association rules," in *Proceedings of the 20th International Conference on Very Large Data Bases*, vol. 1215, 1994, pp. 487–499.
- [24] P. Fournier-Viger, A. Gomariz, M. Campos, and R. Thomas, "Fast vertical mining of sequential patterns using co-occurrence information," in *Advances in Knowledge Discovery and Data Mining: 18th Pacific-Asia Conference*. Springer, 2014, pp. 40–52.
- [25] P. Fournier-Viger, A. Gomariz, M. Šebek, and M. Hlosta, "Vgen: Fast vertical mining of sequential generator patterns," in *Data Warehousing and Knowledge Discovery: 16th International Conference*. Springer, 2014, pp. 476–488.
- [26] Y. Yang, W. Ren, and S. Li, "Hyperlogic: Enhancing diversity and accuracy in rule learning with hypernets," *Advances in Neural Information Processing Systems*, vol. 37, pp. 3564–3587, 2024.
- [27] B. C. Bruce, "A model for temporal references and its application in a question answering program," *Artificial Intelligence*, vol. 3, pp. 1–25, 1972.
- [28] A. E. W. Johnson, D. J. Stone, L. A. Celi, and T. J. Pollard, "The mimic code repository: Enabling reproducibility in critical care research," *Journal of the American Medical Informatics Association*, vol. 25, no. 1, pp. 32–39, 2018.
- [29] S. S. Virani, L. K. Newby, S. V. Arnold, V. Bittner, L. C. Brewer, S. H. Demeter, D. L. Dixon, W. F. Fearon, B. Hess, H. M. Johnson *et al.*, "2023 aha/acc/accp/asnpc/nla/pcna guideline for the management of patients with chronic coronary disease: a report of the american heart association/american college of cardiology joint committee on clinical practice guidelines," *Journal of the American College of Cardiology*, vol. 82, no. 9, pp. 833–955, 2023.

APPENDIX

A. Experimental Results of Real-World Datasets

Results from baseline and our models on four real world medical datasets are present.

1) *AKI Dataset*: The rules and reasoning assessments conducted by the TELLER, CLNN, CLUSTER, and HRTTP models on the AKI dataset are presented in Tables V, VI, VII, and VIII.

2) *Stroke Dataset*: The rules and reasoning assessments conducted by the TELLER, CLNN, CLUSTER, and HRTTP models on the Stroke dataset are presented in Tables IX, X, XI, and XII.

3) *Sepsis Dataset*: The rules and reasoning assessments conducted by the TELLER, CLNN, CLUSTER, and HRTTP models on the Sepsis dataset are presented in Tables XIII, XIV, XV, and XVI.

4) *CAD Dataset*: The rules and reasoning assessments conducted by the TELLER, CLNN, CLUSTER, and HRTTP models on the CAD dataset are presented in Tables XVII, XVIII, XIX, and XX.

TABLE V
TELLER RULES ON THE AKI DATASET.

No.	Rule	Weight	Correctness
1	Hemoglobin Low \rightarrow Phase III	0.4418	correct
2	BUN High \rightarrow Phase III	0.2973	incorrect
3	Heart Rate High \rightarrow Phase III	0.2923	correct
4	WBC High \rightarrow Phase III	0.2002	correct
5	Glucosenserum High \rightarrow Phase III	0.1545	correct

TABLE VI
CLNN RULES ON THE AKI DATASET.

No.	Rule	Weight	Correctness
1	c_PTT High - c_Potassiumserum High > 0	0.73	correct
2	c_PTT High - c_ALT Low > -0.05	0.72	correct
3	c_PTT High - c_C Reactive Protein CRP High > -0.22	0.71	correct
4	c_BUN Low - c_Prothrombin time High > 0.08	0.71	incorrect
5	c_BUN Low - c_Lactic Acid High > 0	0.70	correct
6	c_Lactic Acid High - c_AST Low > 0	0.70	correct

TABLE VII
CLUSTER RULES ON THE AKI DATASET.

No.	Rule	Correctness
1	PTT High after ALT Low	incorrect
2	Anion gap High before Total Bilirubin High	correct
3	Arterial CO2 Pressure High before ALT Low	correct
4	Anion gap High after PH Arterial Low	correct
5	WBC High before PH Arterial Low	correct
6	PTT Low equal Albumin High	incorrect
7	Anion gap Low after C Reactive Protein CRP High	correct
8	PTT High before Prothrombin time Low	incorrect
9	Anion gap High after Heart Rate High	correct
10	PTT High equal BUN Low	incorrect
11	Sodiumserum Low before Hemoglobin High	correct
12	ALT High after BUN High	correct
13	PH Arterial Low before PTT Low	correct
14	Glucosenserum Low after BUN Low	incorrect
15	WBC High before BUN High	correct
16	Anion gap High equal Anion gap Low	incorrect
17	WBC High equal Potassiumserum High	incorrect
18	Heart Rate High after Total Bilirubin High	correct
19	Prothrombin time Low before ALT Low	incorrect
20	Hemoglobin Low before ALT Low	incorrect

TABLE VIII
HRTPP RULES ON THE AKI DATASET.

No.	Rule	Weight	Correctness
1	BUN High before Arterial O2 Saturation Low → Phase III	1.5478	correct
2	Prothrombin time High before ALT Low → Phase III	1.4121	correct
3	Prothrombin time High and Anion gap High → Phase III	0.8598	correct
4	PTT High before Chlorideserum High → Phase III	0.6883	correct
5	Prothrombin time High and ALT Low → Phase III	0.6129	correct
6	AST High → Phase III	0.5802	correct
7	Chlorideserum Low equal Prothrombin time High → Phase III	0.0572	correct
8	Anion gap Low and Prothrombin time High → Phase III	0.0555	correct
9	Sodiumserum High equal PTT High → Phase III	0.0176	correct
10	BUN High equal Hemoglobin Low → Phase III	0.0084	correct

TABLE IX
TELLER RULES ON THE STROKE DATASET.

No.	Rule	Weight	Correctness
1	Temperature Fahrenheit High → Highly unconscious	0.7287	incorrect
2	Respiratory Rate High → Highly unconscious	0.2787	correct
3	Hematocrit Low → Highly unconscious	0.1373	correct
4	Arterial Blood Pressure systolic High → Highly unconscious	-0.1965	correct
5	Temperature Fahrenheit High → Highly unconscious	-0.4720	correct

TABLE X
CLNN RULES ON THE STROKE DATASET.

No.	Rule	Weight	Correctness
1	c_Respiratory Rate High - c_Highly unconscious > -0.02	1.07	correct
2	c_Glucose High - c_Highly unconscious > -0.86	1.03	correct
3	c_Glucose High - c_Anion gap Low > 1.05	1.03	correct
4	c_Arterial Blood Pressure systolic High - c_O2 saturation pulseoxymetry Low > 0.00	0.99	correct
5	c_Hematocrit High - c_Respiratory Rate High > 0.16	0.97	incorrect
6	c_BUN Low - c_Respiratory Rate High > 0.30	0.97	incorrect
7	c_Temperature Fahrenheit Low - c_Respiratory Rate High > 0.10	0.97	correct
8	c_Respiratory Rate High - c_BUN Low > -0.76	0.96	correct
9	c_Temperature Fahrenheit High - c_Creatinine Low > -0.11	0.88	correct
10	c_Anion gap High - c_Arterial Blood Pressure systolic High > 0.21	0.87	incorrect

TABLE XI
CLUSTER RULES ON THE STROKE DATASET.

No.	Rule	Correctness
1	Arterial Blood Pressure systolic High after INR High	correct
2	Chloride High equal BUN High	correct
3	O2 saturation pulseoxymetry Low after Arterial O2 pressure Low	correct
4	Arterial CO2 Pressure Low before Creatinine Low	incorrect
5	Arterial Blood Pressure diastolic High equal Hemoglobin High	correct
6	HCO3 Low after Potassium Low	incorrect
7	Hematocrit Low after Arterial Blood Pressure diastolic High	incorrect
8	Arterial Base Excess High equal Glucose Low	correct
9	Heart Rate High after Arterial Blood Pressure systolic Low	incorrect
10	White Blood Cells High equal Arterial Blood Pressure diastolic High	correct
11	Respiratory Rate High equal Arterial CO2 Pressure High	correct
12	Glucose High before Arterial Base Excess High	correct
13	Respiratory Rate Low equal Chloride Low	incorrect
14	White Blood Cells Low after Hemoglobin High	incorrect
15	Chloride High equal HCO3 Low	correct
16	HCO3 Low before Heart Rate Low	correct
17	O2 saturation pulseoxymetry Low before Hematocrit Low	correct
18	Heart Rate High equal Hematocrit Low	correct
19	Platelet Count Low equal Potassium High	incorrect
20	Arterial CO2 Pressure Low before Sodium Low	correct

TABLE XII
HRTPP RULES ON THE STROKE DATASET.

No.	Rule	Weight	Correctness
1	Temperature Fahrenheit High and Hemoglobin High → Highly unconscious	3.7855	correct
2	Temperature Fahrenheit High → Highly unconscious	1.5625	correct
3	Temperature Fahrenheit High → Highly unconscious	1.5625	correct
4	HCO3 Low equal Temperature Fahrenheit High → Highly unconscious	1.2197	correct
5	Glucose High before Respiratory Rate Low → Highly unconscious	1.0801	correct
6	Arterial Blood Pressure mean Low and Arterial Blood Pressure systolic High → Highly unconscious	0.9993	correct
7	Arterial Blood Pressure systolic High before Creatinine High → Highly unconscious	0.7416	correct
8	Creatinine High equal PTT High → Highly unconscious	0.6306	correct
9	Temperature Fahrenheit High equal Chloride High → Highly unconscious	0.5012	correct

TABLE XIII
TELLER RULES ON THE SEPSIS DATASET.

No.	Rule	Weight	Correctness
1	PTT High → Low Urine	0.0953	correct
2	Platelet Count High → Low Urine	0.0909	incorrect
3	Hemoglobin Low → Low Urine	0.0898	correct
4	Respiratory Rate High → Low Urine	0.0865	correct

TABLE XIV
CLNN RULES ON THE SEPSIS DATASET.

No.	Rule	Weight	Correctness
1	c_Low Urine - c_Arterial Blood Pressure diastolic Low > 0	0.80	correct
2	c_Heart Rate High - c_Hemoglobin High > -0.03	0.78	incorrect
3	c_Arterial Blood Pressure diastolic Low - c_ALT High > -0.06	0.75	correct
4	c_Heart Rate High - c_Arterial Base Excess High > -0.09	0.75	correct
5	c_Arterial Blood Pressure diastolic Low - c_C Reactive Protein High > -0.13	0.74	correct
6	c_Arterial Blood Pressure diastolic Low - c_Hemoglobin High > -0.17	0.73	incorrect
7	c_BUN Low - c_Respiratory Rate High > 0.27	0.68	incorrect
8	c_Heart Rate High - c_C Reactive Protein High > -0.17	0.61	correct
9	c_Heart Rate High - c_Glucose Low > -0.18	0.52	correct

TABLE XV
CLUSTER RULES ON THE SEPSIS DATASET.

No.	Rule	Correctness
1	Arterial Blood Pressure diastolic High after Potassium High	correct
2	Total Bilirubin High equal Temperature Celsius Low	incorrect
3	SpO2 Desat Limit Low after Total Bilirubin Low	correct
4	HCO3 Low after Glucose Low	correct
5	Platelet Count Low after Sodium Low	correct
6	Respiratory Rate High before Arterial CO2 Pressure High	incorrect
7	Prothrombin time High before PTT Low	correct
8	Arterial CO2 Pressure Low before Venous O2 Pressure High	correct
9	Potassium High equal Hemoglobin High	incorrect
10	Hemoglobin High equal Total Bilirubin Low	correct
11	SpO2 Desat Limit Low before Hemoglobin Low	incorrect
12	ALT High before AST Low	incorrect
13	Hemoglobin Low before INR Low	incorrect
14	Arterial Blood Pressure mean High after BUN Low	correct
15	Total Bilirubin High before D-Dimer High	incorrect
16	HCO3 Low before Chloride Low	correct
17	SpO2 Desat Limit Low before SpO2 Desat Limit High	correct
18	Hemoglobin Low equal INR High	incorrect
19	SpO2 Desat Limit Low after Fibrinogen High	correct
20	Respiratory Rate Low equal Hemoglobin High	incorrect

TABLE XVI
HRTPP RULES ON THE SEPSIS DATASET.

No.	Rule	Weight	Correctness
1	Potassium Low equal Lactic Acid High → Low Urine	1.4875	correct
2	Respiratory Rate High and HCO3 Low → Low Urine	1.4736	correct
3	Lactic Acid High equal PH Low → Low Urine	1.3934	correct
4	PH Low before Potassium Low → Low Urine	1.221	correct
5	HCO3 Low equal ALT High → Low Urine	1.1394	correct
6	Heart Rate High equal Arterial Blood Pressure diastolic Low → Low Urine	1.0613	correct
7	BUN Low and Respiratory Rate High → Low Urine	0.8878	incorrect
8	Fibrinogen Low equal Respiratory Rate High → Low Urine	0.7745	correct
9	Magnesium High before Respiratory Rate High → Low Urine	0.7687	incorrect
10	Lactic Acid High equal PTT High → Low Urine	0.5762	correct

TABLE XVII
TELLER RULES ON THE CAD DATASET.

No.	Rule	Weight	Correctness
1	Respiratory Rate High → Dead	0.2859	Correct
2	Arterial Blood Pressure diastolic Low → Dead	0.2202	Correct
3	Heart Rate High → Dead	0.1614	Correct
4	Arterial Blood Pressure mean Low → Dead	0.1400	Correct
5	O2 saturation pulseoxymetry Low → Dead	0.1283	Incorrect

TABLE XVIII
CLNN RULES ON THE CAD DATASET.

No.	Rule	Weight	Correctness
1	c_Glucose High - c_Dead > -0.25	1.03	Correct
2	c_BUN High - c_Dead > -0.63	1.01	Correct
3	c_INR Low - c_BUN High > 0.01	0.99	Incorrect
4	c_Glucose High - c_AST Low > -0.08	0.99	Incorrect
5	c_Albumin High - c_Glucose High > 0.02	0.97	Correct
6	c_BUN High - c_C-Reactive-Protein High > -0.14	0.96	Correct
7	c_Brain Natiuretic Peptide High - c_BUN High > 0.41	0.94	Correct

TABLE XIX
CLUSTER RULES ON THE CAD DATASET.

No.	Rule	Correctness
1	BUN Low equal Lactic Acid Low	Incorrect
2	Hemoglobin High equal Hematocrit High	Incorrect
3	Brain Natiuretic Peptide High after ALT Low	Correct
4	Heart Rate High before AST Low	Correct
5	Calcium ionized High equal Total Bilirubin High	Incorrect
6	CK-MB fraction High equal Calcium ionized Low	Correct
7	Calcium ionized Low equal Cholesterol High	Correct
8	Temperature Low equal Hemoglobin High	Correct
9	Hematocrit Low equal Total Bilirubin Low	Incorrect
10	Glucose Low before Anion gap Low	Incorrect
11	Temperature Low equal INR High	Correct
12	Heart Rate Low before CK-MB fraction High	Correct
13	Arterial Blood Pressure diastolic Low after Anion gap Low	Correct
14	AST Low equal INR Low	Incorrect
15	CK Low after CK High	Incorrect
16	Platelet Count High equal White Blood Cells Low	Correct
17	Heart Rate Low equal Lactic Acid Low	Incorrect
18	Potassium Low equal Total Bilirubin Low	Correct
19	O2 saturation pulseoxymetry High equal Albumin High	Incorrect
20	Temperature High before Cholesterol High	Correct

TABLE XX
HRTPP RULES ON THE CAD DATASET.

No.	Rule	Weight	Correctness
1	Heart Rate Low equal Arterial Blood Pressure diastolic High → Dead	2.4073	Correct
2	Anion gap High before Heart Rate Low → Dead	1.7742	Correct
3	Heart Rate Low equal Potassium High → Dead	1.6257	Correct
4	Potassium Low before O2 saturation pulseoxymetry Low → Dead	1.3959	Correct
5	Respiratory Rate Low before Potassium High → Dead	1.1533	Correct
6	Arterial Blood Pressure mean Low before Arterial Blood Pressure diastolic Low → Dead	1.1312	Correct
7	Anion gap Low equal O2 saturation pulseoxymetry Low → Dead	1.1303	Correct
8	Glucose Low equal Arterial Blood Pressure systolic Low → Dead	0.5603	Correct
9	Heart Rate Low equal INR High → Dead	0.4213	Correct
10	Temperature High and Respiratory Rate High → Dead	0.3194	Correct

B. Ablation Experiment of the Two-Phase Mining Strategy

In the rule mining module, we propose a two-phase mining strategy to enhance the stability and accuracy of rule extraction. To assess its impact, we compare the accuracy of rule extraction with and without this strategy. Table XXI illustrates the improvement in rule accuracy when the two-phase mining strategy is applied. The experimental results demonstrate that this strategy significantly enhances rule extraction precision, further validating its effectiveness in medical event modeling.

TABLE XXI
RULE ACCURACY OF DIFFERENT MINING STRATEGIES.

	AKI	Stroke	Sepsis	CAD
HRTPP w/o two phase mining	80%	80%	71.42%	70%
HRTPP with two phase mining	100%	100%	80%	100%

The experimental results show that the two-phase mining strategy optimizes the precision of the rules in different disease scenarios, enhancing the interpretability of the model. Specifically, in the AKI, Stroke, and CAD datasets, rule accuracy reaches 100%, indicating that this strategy effectively improves the reliability of rule extraction. In the Sepsis dataset, although the accuracy improvement is relatively smaller (from 71.42% to 80%), it still confirms the applicability of this approach to complex medical conditions. These findings suggest that by leveraging point process modeling and an optimized rule mining strategy, we can develop a more stable and interpretable medical event prediction model, providing more reliable support for clinical decision-making.